Structural Engineering and Mechanics, *Vol. 66, No. 3 (2018) 305-315*
DOI: https://doi.org/10.12989/sem.2018.66.3.305

An algorithm to simulate the nonlinear behavior of RC 1D structural members under monotonic or cyclic combined loading

Fatemeh Nouban[a] and Kabir Sadeghi*

Department of Civil Engineering, Near East University, Near East Boulevard, ZIP: 99138, Nicosia, North Cyprus, via Mersin 10, Turkey

(Received December 25, 2017, Revised February 21, 2018, Accepted February 22, 2018)

Abstract. Interaction of lateral loading, combined with axial force needs to be determined with care in reinforced concrete (RC) one-dimensional structural members (1D SMs) such as beam-columns (BCs) and columns. RC 1D SMs under heavy axial loading are known to fail by brittle mode and small lateral displacements. In this paper, a macro element-based algorithm is proposed to analyze the RC 1D SMs under monotonic or cyclic combined loading. The 1D SMs are discretized into macro-elements (MEs) located between the critical sections and the inflection points. The critical sections are discretized into fixed rectangular finite elements (FRFE). The nonlinear behavior of confined and unconfined concretes and steel elements are considered in the proposed algorithm. The proposed algorithm has been validated by the results of experimental tests carried out on full-scale RC structural members. The evolution of ultimate strain at extreme compression fiber of a rectangular RC section for different orientations of lateral loading shows that the ultimate strain decreases with increasing the axial force. In the examined cases, this ultimate strain ranges from 0.0024 to 0.0038. Therefore, the 0.003 value given by ACI-318 code for ultimate strain, is not conservative and valid for the combined load cases with significant values of axial force (i.e. for the axial forces heavier than 70% of the ultimate axial force).

Keywords: reinforced concrete; 1D structural members; beam-columns; columns; simulation; monotonic; cyclic; combined loading

1. Introduction

The Conventional design of buildings largely employs the linear analysis of structures. The interaction of lateral loading or uniaxial bending moment (UBM) or biaxial bending moment (BBM), combined with axial force in RC 1D SMs, needs to be determined with care. RC 1D SMs are known to fail by brittle mode at peak axial loads and small lateral displacements (Sharma *et al.* 2014).

The behavior of 1D SMs has been investigated by several researchers. Pham *et al.* (2010) presented a new finite Timoshenko beam element with a model for ultimate load computation of RC frames. The model combines the descriptions of the diffuse plastic failure in the BC followed by the creation of plastic hinges due to the failure or collapse of the concrete and or the reinforcements.

A modified multi-scale analysis is performed in order to identify the parameters for the stress-resultant-based macro model. Special attention is paid to the influence of the axial force on the bending moment-rotation response. Mashaly *et al.* (2011) proposed a BC model for seismic analysis of RC frames. This model is a simplified version of the flexibility-based fiber models, which is based on dividing the member length into small segments and dividing the cross section of each segment into concrete and steel fibers. In this model, only the two end sections are subdivided into fibers. Uniaxial material models of steel and concrete under cyclic loading are assigned to the cross-section's fibers. Morfidis *et al.* (2014) presented an inelastic model based on the nonlinear material response and the interaction relation between axial forces and bending moments of a BC member. The model is simple and is easy to implement in standard structural analysis codes, and avoids the complexities of expensive alternative analyses based on finite-element computations.

Plastic hinges play a significant role in the behavioral response of BCs. In the majority of BC sub-assembly tests, the plastic hinges form in beams rather than in the columns. In RC structures, beam column connections are one of the most critical regions in areas with seismic susceptibility. Proper anchorage of reinforcements is vital to enhance the performance of beam column joints. Various models have been proposed by several researchers for predicting the exterior RC beam column joint strength. Most of these models were calibrated and verified with some limited experimental database. Among them, Parate and Kumar (2016) presented a detailed investigation of several analytical models to predict the shear strength of exterior beam column joint. The study shows the effect of each governing parameter on the joint's shear strength predicted by various models.

During the analysis and design of reinforced concrete frames, beam column joints are sometimes assumed as rigid. This simplifying assumption can be unsafe because it is likely to affect the distributions of internal forces and moments, reduce drift and increase the overall load-

*Corresponding author, Professor
E-mail: kabir.sadeghi@neu.edu.tr
[a]Assistant Professor
E-mail: fatemeh.nouban@neu.edu.tr

ISSN: 1225-4568 (Print), 1598-6217 (Online)

carrying capacity of the frame.

The behavior of RC 1D SMs subjected to combined loading has been studied by several researchers. Among them, Yen (1991) considered the longitudinal reinforcement percentage and the neutral axis (NA) location as two main variables and proposed a method to analyze the RC sections subjected to biaxial bending moment (BBM). Several simplifications, employed in this method, have an unfavorable effect on the accuracy of the results. Yau *et al.* (1993) considered the longitudinal reinforcement percentage, and the distance between the point having maximum compressive stress and NA, as two main variables and proposed a method to analyze the ultimate strength of the RC sections subjected to BBM. Amziane and Dubé (2008) proposed an algorithm to simulate RC structures under the combined uniaxial cyclic bending and axial load. They employed this simulation algorithm to quantify the global structural damage based on the assessment of local material damage. Massumi and Monavari (2013) have proposed an energy-based method to obtain the target displacement for RC frames subjected to cyclic combined loading assuming that the capacity for absorbing the energy of the structures for both the pushover and cyclic analyses are equal. Massumi and Badkoubeh (2015) have presented a numerical procedure that provides the ultimate curvature and moment domains for the rectangular and circular cross-sections of the RC columns subjected to biaxial bending and axial loading. They have proposed a dimensionless formula that can be used for the sections with similar normalized geometric and mechanical properties.

To analyze the RC sections subjected to cyclic biaxial bending moment and axial loading (BBMAL), the direct search procedure to determine the strain equilibrium plane is employed. In this case, the section is discretized into FRFE. This method can be used in both cyclic and monotonic loading cases.

In this paper, an algorithm to simulate numerically the behavior of RC 1D SMs subjected to cyclic combined loading including the inclined lateral force at any direction perpendicular to the longitudinal axis of 1D SM, BBM or UBM together with the axial loading. In order to simulate the RC structural members under cyclic loading, the FRFE discretization type is adapted to discretize the critical sections.

The main advantages of employing the proposed algorithm, compared to those given previously by other researchers, can be summarized as follows:

• The aim of most researchers is to determine the ultimate strength of the 1D SMs while utilizing the proposed algorithm, the instantaneous strength of the 1D SMs together with much more information is calculated at any stage of loading from the intact state up to the failure of the 1D SMs.

• In most researches, simplified strain-stress models for concrete and reinforcement are used, while the proposed algorithm employs the nonlinear models adapted to the actual behavior of the materials including the loss of concrete cover and the failure of confined concrete elements.

• Contrary to some models, the proposed algorithm allows the user to cross over the peaks and inflection points when calculating the 1D SM's response (see Fig. 6). By applying the proposed convergence search method to determine the equilibrium state, the convergence is guaranteed for any loading case.

2. Structure of the proposed algorithm

2.1 Overall specifications

In the case that the 1D SM is a beam-column, it is decomposed into four Macro-Elements (MEs) located between the critical sections (i.e.,: maxim moments at the mid-span and at the supports) and the inflection points. Due to symmetry, there are only 2 sets of MEs with different lengths instead of four MEs (2 identical shorter MEs and 2 identical longer MEs). In the case that the 1D SM is a column, it is decomposed into two MEs located between the critical sections (i.e.: maxim moments at the two ends of the column) and the inflection point. A Macro-Element (ME) is defined as a fixed end-free end 1D SM subjected to combined loading (i.e.: a cyclic biaxial bending moment or inclined lateral load together with axial force). Then the nonlinear behavior of MEs is analyzed and the MEs are assembled to form the 1D SM. An identical value of shear force in inflection point is applied to the ends of the MEs. By increasing the value of this shear force, the response of the 1D SMs at the fixed ends of MEs are calculated, while this shear force is increased from zero up to the failure of the member.

In the case that the 1D SM is a BC it can easily be shown from a consideration of bending moments in a fixed end BC (for the cases of uniformly distributed loading and also in the case that one-way or two-way slabs are attached to the BC) that the points of inflection would be located at a distance of 0.21 L from each end, where L represents the span length of the BC. In the practical cases of partial fixity, as a reasonable approximation, the points of inflection may be assumed to lie at one-tenth of the span length from each end joint (Norris and Wilbur, 1960). In the case that the 1D SM is a column under combined load including the lateral load, the inflection point is considered at the middle of the column.

In the proposed algorithm, the strain distributions at the sections are taken up to form a plane, which remains a plane during deformation due to loading. Uniaxial constitutive laws are used to simulate the stresses of the concrete and reinforcement elements. For the compressive confined and unconfined concrete elements the monotonic and cyclic constitutive laws proposed by Sadeghi and Nouban (2017), based on the experimental tests of Sadeghi (2001), have been used. Note that the highly-theoretical-based concrete constitutive laws proposed by some researchers such as Lavassani *et al.* (2009) and Tasnimi and Lavasani (2011) require complicated expensive test input data, while the applied constitutive law in this research, needs the design characteristic strength of unconfined concrete together with the confining stirrups' specifications and gives acceptable results adapted to the experimental results. For reinforcements, the cyclic model proposed by

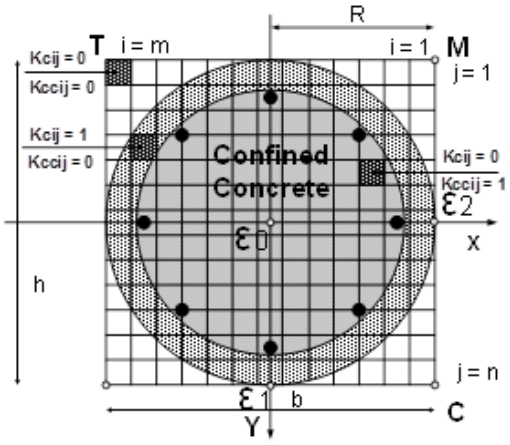

Fig. 1 FRFE discretization of a 1D SM's section

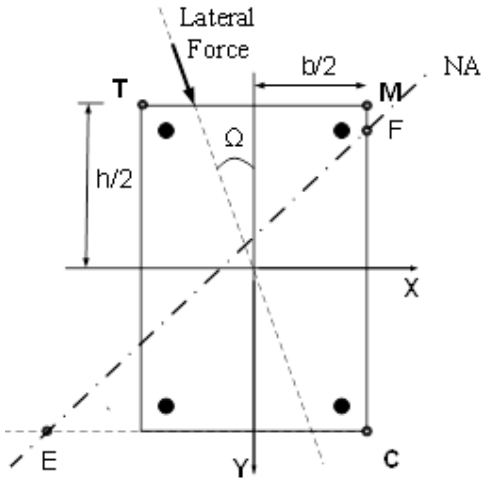

Fig. 2 Situation of lateral load and NA on a 1D SM's section

Park *et al.* (1972) have been employed. To simulate the behavior of tensile stress in concrete elements, a linear stress-strain model up to the tensile strength of concrete is employed. To limit the strains to the maximum values of the compressive strains in unconfined and confined concretes, the formulas proposed by CEB Code (1978) and Sheikh (1982) have been used, respectively. These formulas are employed to simulate the loss of concrete cover and the failure of confined concrete. Since the ACI318-11 criteria are based on the perfect bond assumption and also in most of the simulations the perfect bond between the reinforcements and concrete is assumed (Hashemi and Vaghefi 2015), in the proposed simulation, the bond between the longitudinal reinforcements and concrete is assumed as perfect bond.

A "strain plane control process" method is adapted in the proposed algorithm to calculate the strains and then the stresses at the centers of the concrete and steel elements. A system of three as in three variables, applying a triple iteration process and a proposed difference-based Bisection numerical search method over the strains, is solved to verify the equilibrium state in each section. The equilibrium is justified over each section considering the law of "plane sections remain plane during deformation". The computations are founded on the cyclic nonlinear behavior of concrete and reinforcement elements. In each concrete element ij (i, j) and in each steel element k, the stresses are determined in function of strains (ε). Different loading-unloading stages are determined by means of saving the last three strain values. In order to reach equilibrium, three characteristic strains comprising: ε_C (the strain of the point C with the maximum compressive stress in the section), ε_T (the strain of the point T with the maximum tensile stress in the section) and ε_M (the strain in the point M located at another corner of the section), as shown in Figs. 1 and 2, are employed as three main variables. For non-rectangular section cases the points C, T and M are located out of the structural member section and located on the discretizing mesh boundaries.

2.2 Adapted discretization method

The critical sections of RC 1D SMs are discretized into FRFE as shown in Fig. 1. In the proposed algorithm the FRFE discretization type with the fixed locations has been applied. This type of discretization, allows the loading-unloading path to be continuously followed up in monotonic and cyclic loading cases. The center of the mesh is located in the geometry center of the cross-section. The orientation angles Ω is the angle between the lateral force and the y-axis of the section, as illustrated in Fig. 2.

2.3 Equilibrium principles

The equilibrium of each section is achieved by equating the internal and external forces and moments

$$N_{ext} = N_{int} \tag{1}$$

$$Mx_{ext} = Mx_{int} \tag{2}$$

$$My_{ext} = My_{int} \tag{3}$$

Eqs. (4) to (6) present the internal efforts

$$N_{int} = \sum_{i}^{m}\sum_{j}^{n} Kcc_{ij}\,.\,\sigma cc_{ij}.A_{ij} + \sum_{i}^{m}\sum_{j}^{n} Kc_{ij}.\sigma c_{ij}.A_{ij} + \sum_{k}^{ns} \sigma s_k.As_k \tag{4}$$

$$Mx_{int} = \sum_{i}^{m}\sum_{j}^{n} Kcc_{ij}\,.\,\sigma cc_{ij}.y_{ij}.A_{ij} + \sum_{i}^{m}\sum_{j}^{n} Kc_{ij}.\sigma c_{ij}.y_{ij}\,.A_{ij} + \sum_{k}^{ns} \sigma s_k.y_k\,.As_k \tag{5}$$

$$My_{int} = \sum_{i}^{m}\sum_{j}^{n} Kcc_{ij}\,.\,\sigma cc_{ij}.\,x_{ij}.\,A_{ij} + \sum_{i}^{m}\sum_{j}^{n} Kc_{ij}.\,\sigma c_{ij}.\,x_{ij}\,.\,A_{ij} + \sum_{k}^{ns} \sigma s_k.\,x_k\,.\,As_k \quad (6)$$

Where:

N_{ext}: external axial force,

N_{int}: internal axial force,

Mx_{ext}: external bending moment about x-axis (see Figs. 1 and 2),

My_{ext}: external bending moment about y-axis (see Figs. 1 and 2),

Mx_{int}: internal bending moment about x-axis,

My_{int}: internal bending moment about y-axis,

σcc_{ij}: stress in confined concrete element ij,

σc_{ij}: stress in unconfined concrete element ij,

σs_k: stress in steel element k,

A_{ij}: area of concrete element ij,

As_k: area of steel element k,

Kccij: material existence indicator for confined concrete element ij (Kccij = 1, indicate the existence of a confined concrete element ij),

Kcij: material existence indicator for unconfined concrete element ij (Kcij = 1, indicate the existence of an unconfined concrete element ij),

ns: the total number of longitudinal steel bars in the section,

m: number of elements in the y-direction (maximum value of i),

n: number of elements in the x-direction (maximum value of j).

Kccij = 0 and Kcij = 0 are employed to indicate a failed element or an imaginary element located out of the section, or in the hollow zone of the section (Sadeghi 1995) (see Fig. 1).

The total external and internal bending moments "M_{ext} and M_{int}" are determined as follows

$$M_{ext} = [(Mx_{ext})^2 + (My_{ext})^2]^{1/2} \quad (7)$$

$$M_{int} = [(Mx_{int})^2 + (My_{int})^2]^{1/2} \quad (8)$$

The equilibrium state is established by finding the resolution of a system with three equations and three variables by means of a triple iteration process and applying a proposed difference-based Bisection numerical research method over the characteristic strains.

2.4 Calculation of strains

The strains in the confined and unconfined concrete elements "ε_{ij}" and steel elements "εs_k" are determined as follows

$$\varepsilon_{ij} = \varepsilon_0 + \phi_x(x_{ij} - x_0) + \phi_y(y_{ij} - y_0) \quad (9)$$

$$\varepsilon s_k = \varepsilon_0 + \phi_x(xs_k - x_0) + \phi_y(ys_k - y_0) \quad (10)$$

With

$$\varepsilon_0 = \varepsilon_C - \phi_x\left(\frac{b}{2}\right) - \phi_y(h/2) \quad (11)$$

Where:

ε_0: strain at the center of gravity of the section (see Fig. 1),

(x_{ij}, y_{ij}) : coordinates of the center of gravity of concrete elements,

(x_{sk}, y_{sk}): coordinates of the center of gravity of steel elements,

(x_0, y_0): coordinates of the center of gravity of the section,

ϕ_x: curvatures in the x-direction,

ϕ_y: curvatures in the y-direction.

2.5 Calculation of curvatures

The curvatures in the x- and y-directions are determined by employing the following equations

$$\phi_x = \frac{(\varepsilon_2 - \varepsilon_0)}{(b/2)} \quad (12)$$

$$\phi_y = \frac{(\varepsilon_1 - \varepsilon_0)}{(h/2)} \quad (13)$$

With

$$\varepsilon_2 = \frac{\varepsilon_C + \varepsilon_M}{2} \quad (14)$$

$$\varepsilon_1 = \varepsilon_C + \frac{\varepsilon_T}{2} - \frac{\varepsilon_M}{2} \quad (15)$$

Where

$$\varepsilon_C = \varepsilon_0 + \phi_x(b/2) + \phi_y(h/2) \quad (16)$$

$$\varepsilon_T = \varepsilon_0 - \phi_x(b/2) - \phi_y(h/2) \quad (17)$$

$$\varepsilon_M = \varepsilon_0 + \phi_x(b/2) - \phi_y(h/2) \quad (18)$$

The b and h dimensions, as well as the locations of ε_1 and ε_2, are illustrated in Fig. 1.

The overall curvature "ϕ" is given as

$$\phi = \sqrt{{\phi_x}^2 + {\phi_y}^2} \quad (19)$$

2.6 Neutral axis location

The coordinates of NA intersections with the axes of x and y are calculated using the following equations

$$x_n = \frac{b}{2} + \left(\frac{h}{2}\right)\left(\frac{\phi_y}{\phi_x}\right) - \frac{\varepsilon_C}{\phi_x} \quad (20)$$

$$y_n = \frac{h}{2} + \left(\frac{b}{2}\right)\left(\frac{\phi_x}{\phi_y}\right) - \frac{\varepsilon_C}{\phi_y} \quad (21)$$

The neutral axis line passes through the points E(x_n, 0) and F(0, y_n) (see Fig. 2).

2.7 ME loading history recording

Every loading step is saved and is compared to the two preceding steps.

During every loading step p, on each critical section l, for the imposed force (moment) "$M_{ext}(p,l)$" or imposed displacement (curvature) "$\phi(p,l)$", the difference factors "$dM1$ and $dM2$", or "$d\phi1$ and $d\phi2$" are calculated, respectively. The difference factors indicate the loading cases.

2.7.1 For the case of imposing force (moment) on ME

$$dM1 = M_{ext}(p-1,l) - M_{ext}(p-2,l) \quad (22)$$

$$dM2 = M_{ext}(p,l) - M_{ext}(p-1,l) \quad (23)$$

Loading cases are identified as:

• It is a loading case if

$$[dM1 \geq 0 \text{ and } dM2 > 0] \quad (24)$$

• It is an unloading just after a loading case if

$$[dM1 \geq 0 \text{ and } dM2 < 0] \quad (25)$$

• It is an unloading after an unloading case if

$$[dM1 < 0 \text{ and } dM2 < 0] \quad (26)$$

• It is a reloading after unloading case if

$$[dM1 < 0 \text{ and } dM2 > 0] \quad (27)$$

2.7.2 For the case of imposing displacement (curvature) on ME

$$d\phi1 = \phi(p-1,l) - \phi(p-2,l) \quad (28)$$

$$d\phi2 = \phi(p-1,l) - \phi(p-2,l) \quad (29)$$

Loading cases are identified as follows:

• It is a loading case if

$$[d\phi1 \geq 0 \text{ and } d\phi2 > 0] \quad (30)$$

• It is an unloading just after a loading case if

$$[d\phi1 \geq 0 \text{ and } d\phi2 < 0] \quad (31)$$

• It is an unloading after an unloading case if

$$[d\phi1 < 0 \text{ and } d\phi2 < 0] \quad (32)$$

• It is a reloading after unloading case if

$$[d\phi1 < 0 \text{ and } d\phi2 > 0] \quad (33)$$

2.8 Concrete elements loading history recording

During the recording of the loading history, the three last stress and strain values for each concrete element ij are saved to compare with those recorded in the preceding steps. For every concrete element ij discretized on section l, in the step p of loading, the difference factors "$d\varepsilon1$ and $d\varepsilon2$" are calculated.

$$d\varepsilon1 = \varepsilon(p-1,l,i,j) - \varepsilon(p-2,l,i,j) \quad (34)$$

$$d\varepsilon2 = \varepsilon(p,l,i,j) - \varepsilon(p-1,l,i,j) \quad (35)$$

The loading cases on the strain-stress curve of each concrete element are identified by the following conditions:

• It is a loading case if

$$[d\varepsilon1 \geq 0 \text{ and } d\varepsilon2 > 0] \quad (36)$$

• It is an unloading just after a loading case if

$$[d\varepsilon1 \geq 0 \text{ and } d\varepsilon2 < 0] \quad (37)$$

• It is an unloading after an unloading case if

$$[d\varepsilon1 < 0 \text{ and } d\varepsilon2 < 0] \quad (38)$$

• It is a reloading after unloading case if

$$[d\varepsilon1 < 0 \text{ and } d\varepsilon2 > 0] \quad (39)$$

2.9 Recording the steel elements loading history

During the recording of the loading history, the three last stress and strain values for each steel element k are saved to compare with those recorded in the preceding steps. For every steel element k discretized on section l, in the step p of loading, the difference factors "$d\varepsilon1$ and $d\varepsilon2$" are calculated.

$$d\varepsilon1 = \varepsilon(p-1,l,k) - \varepsilon(p-2,l,k) \quad (40)$$

$$d\varepsilon2 = \varepsilon(p,l,k) - \varepsilon(p-1,l,k) \quad (41)$$

These parameters allow fixing the limits given for the iteration process needed to research the equilibrium parameters. The four different typical cases are identified as follows:

• It is a loading case if

$$[d\varepsilon1 \geq 0 \text{ and } d\varepsilon2 > 0] \quad (42)$$

• It is an unloading just after a loading case if

$$[d\varepsilon1 \geq 0 \text{ and } d\varepsilon2 < 0] \quad (43)$$

• It is an unloading after an unloading case if

$$[d\varepsilon1 < 0 \text{ and } d\varepsilon2 < 0] \quad (44)$$

• It is a reloading after unloading case if

$$[d\varepsilon1 < 0 \text{ and } d\varepsilon2 > 0] \quad (45)$$

2.10 Regulating the characteristics strains (ε_C, ε_T and ε_M)

A proposed bisection method is applied to find the equilibrium state in each section of 1D SM that repeatedly bisects an interval and then selects a subinterval in which a root must lie for further processing. The method is applicable for numerically solving the equation $f(x) = 0$ for the real variable x, where f is a continuous function defined on an interval $[a, b]$. The interval $[a, b]$ for the

following strains are $[(\varepsilon_{Cmin}, \varepsilon_{Cmax}]$, $[\varepsilon_{Tmin}, \varepsilon_{Tmax}]$ and $[(\varepsilon_{Mmin}, \varepsilon_{Mmax}]$, respectively (See also Section 2.13.1).

The extreme compressive strain (in point C) (see Figs. 1 and 2)

$$\varepsilon_C = (\varepsilon_{Cmin} + \varepsilon_{Cmax})/2 \quad (46)$$

The extreme tensile strain (in point T) (see Figs. 1 and 2)

$$\varepsilon_T = (\varepsilon_{Tmin} + \varepsilon_{Tmax})/2 \quad (47)$$

The strain in the point M located at the third corner of the section (see Figs. 1 and 2)

$$\varepsilon_M = (\varepsilon_{Mmin} + \varepsilon_{Mmax})/2 \quad (48)$$

The initial values for ε_{Mmin} and ε_{Mmax} can be considered as ε_T and ε_C, respectively.

In loading or reloading cases

$$\varepsilon_T \leq \varepsilon_M \leq \varepsilon_C \quad (49)$$

In unloading cases

$$\varepsilon_T \geq \varepsilon_M \geq \varepsilon_C \quad (50)$$

2.11 Equilibrium verification in equilibrium state

To achieve the equilibrium state, a set of successive iteration processes is followed to satisfy the following three conditions:

2.11.1 Orientation angle verification

The external and internal orientation angles Ω (the angle between the lateral force and the y-axis of the section, as illustrated in Fig. 2) must be balanced. This is verified by an iteration process over the strains of point M (ε_M) for the given values of ε_C and ε_T as demonstrated below

$$\varepsilon_{Mmax} = \varepsilon_M \quad (\text{for } \Omega_{int} > \Omega_{ext}) \quad (51)$$

$$\varepsilon_{Mmin} = \varepsilon_M \quad (\text{for } \Omega_{int} < \Omega_{ext}) \quad (52)$$

In the following trial, an average strain value is employed, as given by the following equation

$$\varepsilon_{M(i+1)} = (\varepsilon_{Mmin(i)} + \varepsilon_{Mmax(i)})/2 \quad (53)$$

The following condition must be satisfied for the orientation angle

$$\Omega_{ext} = \Omega_{int} \quad (54)$$

Where

$$\Omega_{ext} = \Omega = Tan^{-1}(My_{ext}/Mx_{ext}) \quad (55)$$

$$\Omega_{int} = Tan^{-1}(My_{int}/Mx_{int}) \quad (56)$$

2.11.2 Verification of axial forces in equilibrium state

During a second iteration process over the extreme tensile strains at point T (ε_T) for the given value of ε_C, the equilibrium between the external and internal axial forces is verified as illustrated below

$$\varepsilon_{Tmax} = \varepsilon_T \quad (\text{for } N_{int} > N_{ext}) \quad (57)$$

$$\varepsilon_{Tmin} = \varepsilon_T \quad (\text{for } N_{int} < N_{ext}) \quad (58)$$

The average strain value is employed in the following trial

$$\varepsilon_{T(i+1)} = (\varepsilon_{Tmin(i)} + \varepsilon_{Tmax(i)})/2 \quad (59)$$

The following condition must be satisfied for the axial force

$$N_{ext} = N_{int} \quad (60)$$

2.11.3 Verification of bending moments in equilibrium state

During a third iteration process over the extreme compressive strain (in point C), the equilibrium between the external and internal bending moments is verified as shown below

$$\varepsilon_{Cmin} = \varepsilon_C \quad (\text{for } M_{int} > M_{ext}) \quad (61)$$

$$\varepsilon_{Cmax} = \varepsilon_C \quad (\text{for } M_{int} < M_{ext}) \quad (62)$$

The average strain value is employed in the following trial

$$\varepsilon_{C(i+1)} = (\varepsilon_{Cmin(i)} + \varepsilon_{Cmax(i)})/2 \quad (63)$$

The following condition must be satisfied for the bending moment

$$M_{ext} = M_{int} \quad (64)$$

2.12 Convergence tolerances for the equilibrium state

The reasonably accurate convergence tolerances given below are employed in the proposed algorithm for the equilibrium state

$$|\Omega_{ext} - \Omega_{int}| \leq 0.1° \quad (65)$$

$$|N_{ext} - N_{int}| \leq 0.001\,|N_{ext}| \quad (66)$$

$$|M_{ext} - M_{int}| \leq 0.001\,|M_{ext}| \quad (67)$$

2.13 Convergence procedure to achieve the equilibrium state in a section

2.13.1 Applied proposed bisection method

A proposed bisection method (also called the interval halving method, the binary search method, or the dichotomy method) is applied as a root-finding method that repeatedly bisects an interval and then selects a subinterval in which a root must lie for further processing.

The method is applicable for numerically solving the equation $f(x) = 0$ for the real variable x, where f is a continuous function defined on an interval $[a, b]$ which are said to bracket a root. Contrary to the Bisection method of Bolzano $f(a)$ and $f(b)$ have not to have opposite signs. In the Bolzano Bisection method, the product of the functions should be negative and it is a product-based method and approach to the solution from two sides to zero, while the proposed Bisection method is a difference- based

method and approaches to the solution from one side.

At each step, the method divides the interval in two by computing the midpoint $c = (a+b)/2$ of the interval and the value of the function $f(c)$ at that point. The method selects the subinterval that is guaranteed to be a bracket as the new interval to be used in the next step. The process is continued until the interval is sufficiently small or the desired accuracy tolerances achieved.

The input for the method is a continuous function f, an interval $[a, b]$, and the function values $f(a)$ and $f(b)$. Each iteration performs these steps:

1. Calculate c, the midpoint of the interval, $c = a + b/2$.
2. Calculate the function value at the midpoint, $f(c)$.
3. If convergence is satisfactory (that is, c-a is sufficiently small, or $|f(c)|$ is sufficiently small), return c and stop iterating.
4. Examine the value of $f(c)$ and replace either $(a, f(a))$ or $(b, f(b))$ with $(c, f(c))$ so that there is a new c within the new interval.

During the implementation of the method on the computer program, there are problems with finite precision, so there are convergence acceptance tolerance limits of the function under question. Additionally, the difference between a and b is limited by the floating point precision; i.e., as the difference between a and b decreases, at some point, the midpoint of $[a, b]$ will be numerically identical to (within floating point precision of) either a or b.

In the proposed algorithm, the method is written in pseudocode and for the three loops of iteration processes the following variables, function, and tolerances are adapted:

Input:

Function f: $\Omega_{ext} - \Omega_{int}$, endpoint values a, b: ε_{Mmin}, ε_{Mmax}, tolerance (TOL): 0.1°

Function f: $N_{ext} - N_{int}$, endpoint values a, b: ε_{Tmin}, ε_{Tmax}, TOL: $0.001\,|N_{ext}|$

Function f: $M_{ext} - M_{int}$, endpoint values a, b: ε_{Cmin}, ε_{Cmax}, TOL: $0.001\,|M_{ext}|$

Output: value which differs from a root of f(x) = 0 by less than TOL.

2.13.2 Flowchart for the convergence procedure part

Fig. 3 presents the flow chart for the part of the convergence procedure to achieve the equilibrium state in a section of 1D SM.

2.14 Determination of displacements

The traditional double integration method is applicable mainly for the members with the homogeneous material and in the elastic range, it underestimates the deflection in the post-elastic phase. Two options for the calculation of displacements are considered in SMNLAP: "Double Integration Method" (DIM) and "Elastic-Plastic Method" (EPM).

In DIM option, a numerical double integration on ϕ_x and ϕ_y is carried out. In this option, Eqs. (68) to (71) are employed

$$\delta_{xl} = \sum_{i=1}^{i=l} dh\left[\theta_{xi} + \left(\phi_{xi} + 2\phi_{x(i-1)}\right)dh/6\right] \quad (68)$$

$$\delta_{yl} = \sum_{i=1}^{i=l} dh\left[\theta_{yi} + \left(\phi_{yi} + 2\phi_{y(i-1)}\right)dh/6\right] \quad (69)$$

$$\theta_{xl} = \sum_{i=1}^{i=l} dh\left[\left(\phi_{xi} + 2\phi_{x(i-1)}\right)/2\right] \quad (70)$$

$$\theta_{yl} = \sum_{i=1}^{i=l} dh\left[\left(\phi_{yi} + 2\phi_{y(i-1)}\right)/2\right] \quad (71)$$

Where:

dh: L/p (L and p are the length and the number of sections of ME, respectively),

ϕ_{xi}: curvature in x-direction in section i,

ϕ_{yi}: curvature in y-direction in section i,

$\phi_{x(i-1)}$: curvature in x-direction in section $i-1$,

$\phi_{y(i-1)}$: curvature in y-direction in section $i-1$,

δ_{xl}: displacement in x-direction in section l,

δ_{yl}: displacement in y-direction in section l,

θ_{xl}: rotation in x-direction in section l,

θ_{yl}: rotation in y-direction in section l.

The resultant of δ_{xl} and δ_{yl}, projected in the direction of the applied lateral force gives the displacement sought. This method is time-consuming and underestimates the deflection in post-elastic phase in comparison with elastic-plastic method (EPM) proposed by Priestley and Park (1991).

The EPM is based on the evidence that a column is highly affected in the critical zone when a lateral load, UBM or BBM is applied. The main bending effect is due to the curvature registered at critical sections.

In this paper, the column deflections were determined using the EPM that considers mainly the curvature at the critical section and the length of the column in the elastic phase. Immediately following the peak value of the "moment-curvature" (M-ϕ) curve at the critical section, a very important local effect occurs at the critical section where a pseudo-plastic hinge appears. Once the peak has passed, curvature enhancement is concentrated in the critical zone. While in the other regions, the cracks start to be closed and the curvatures decrease rapidly to near zero.

The EPM option (Eqs. (72) and (73)), proposed by Priestley and Park (1991) is preferred when a pseudoplastic hinge appears in a critical section.

$$\delta = \left(\frac{\phi}{3} L^2\right) \qquad (\text{for } \phi \le \phi_p) \quad (72)$$

$$\delta = \left(\frac{\phi_p}{3} L^2\right) + (\phi - \phi_p)(L_p)(L - 0.5\, L_p) \qquad (\text{for } \phi \ge \phi_p) \quad (73)$$

Where:

δ: relative displacement at the end of ME,

ϕ: curvature at critical section,

ϕ_p: curvature when plastic hinge is performed,

L: length of ME,

Lp: length of the plastic hinge.

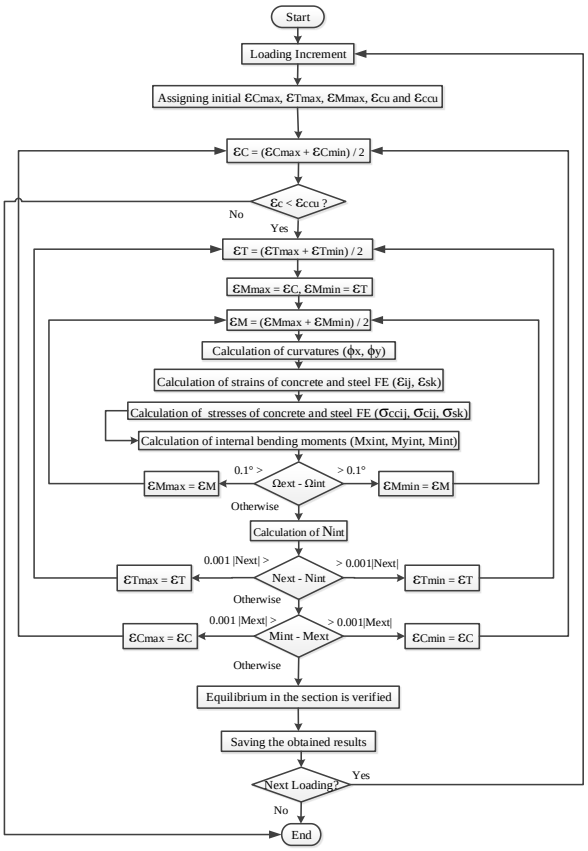

Fig. 3 Convergence procedure to achieve the equilibrium state in a section of 1D SM

2.15 Calculation of equivalent viscous damping ratio

The energy dissipated in a cycle equals the area of the force-displacement (dissipation hysteresis) loop. For reasons of convenience, an equivalent viscous damping, dissipating the same energy per cycle, is employed. Its relative value (relative to the critical damping) is given as an equivalent viscous damping ratio (EVDR) shown by "ξ" as submitted in Eq. (74)

$$\xi = \frac{W_D}{4\,\pi W_S} \tag{74}$$

Where:

W_D: damping energy dissipated per cycle (Area of a hysteresis loop),

W_S: peak elastic energy stored in the secant stiffness system for the same elastic displacement (Area of a triangle).

3. Computer program

A computer program called structural members nonlinear analysis program (SMNLAP) has been prepared by the authors to simulate the response of reinforced concrete 1D SMs subjected to cyclic combined loading including inclined lateral load, UBM or BBM together with the axial loading. The Main sub-programs of SMNLAP are:

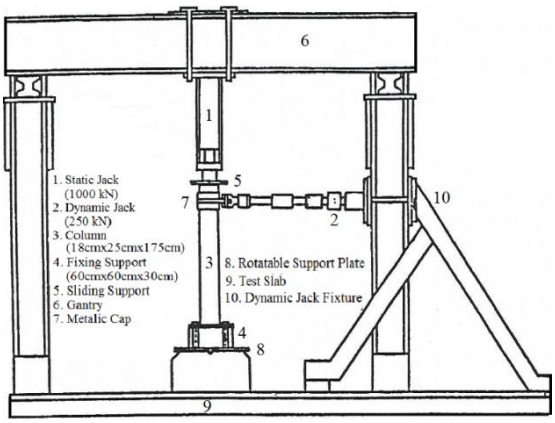

Fig. 4 Overall assemblage of the experimental test performed at the University of Nantes (Sadeghi 1995)

BBCS (biaxial bending column simulation), CCS (confined concrete simulation), UCS (unconfined concrete simulation), RS (reinforcement simulation), NALS (neutral axis location simulation), DS (displacement simulation), BM-AL ID (bending moment-axial load interaction diagram), DSS (damping and stiffness simulation) and DIS (damage index simulation).

SMNLAP is capable of simulating the failure, the internal local behavior of critical sections (strain and stress in concrete and steel elements, NA location, material loss and local damage (Sadeghi and Nouban (2017)) and the external global behavior of the 1D SM (displacement, curvature, damping ratio, stiffness and global damage) (Sadeghi 2011, Sadeghi and Nouban 2016), etc.). The concrete confinement due to the transverse reinforcement and the loss of the concrete cover is also taken into account in SMNLAP.

4. Experimental test data

The proposed algorithm has been validated by the experimental tests performed by Garcia Gonzalez (1990) and Park *et al.* (1972). The Garcia Gonzalez tests were performed at the University of Nantes on full-scale columns under cyclic lateral oriented loading and axial force (CLOLAF), and monotonic lateral oriented loading and axial force (MLOLAF)). The characteristics of the tested physical model are summarized as follows: rectangular section (18 cm × 25 cm), column height = 1.75 m, four longitudinal reinforcements with a diameter of 12 mm (percentage of steel ρ = 1%), concrete of strength f_c' = 42 MPa, stirrups of 6 mm diameter with 9 cm spacing, yield stress of steel bars: Fy = 470 MPa. The column was fixed at the bottom, free at the top. The lateral loads, through different orientation angels Ω (see Fig. 2), were applied to the top of the columns. In this paper, this tested physical model is called "reference model" and its critical section is called "reference section".

The tests were performed for each angle of applied lateral load Ω, ranging between 0º and 90º in 15º steps. Each column was subjected simultaneously to a 500 kN vertical constant loading and a lateral displacement applied

to the top level of the column. The loading was performed employing two jacks as described below:

• A static jack, type LOS DZN-100, having a capacity of 1000 kN with a maximum amplitude of 250 mm that imposed the vertical force. This jack was connected to a control panel, type PK-SRG 5000 with the automatic control of unloading at the point of failure of the column.

• A dynamic jack, type LOS 250, having a capacity of 250 kN that imposed the lateral displacement.

These two jacks were installed on the test gantry and were fed by a controlled hydraulic system.

Fig. 4 illustrates the overall assemblage of the experimental test.

The column under test was connected rigidly to a support fixed to the test platform, using a circular steel plate that can rotate about the vertical axis. The rotatable circular plate allows the orientation of the column in the direction required to apply the lateral force. The dynamic jack was fixed horizontally to the gantry and was supported by two oblique legs that were prestressed to the test slab in two opposite directions in the plane of the gantry. A hooped elastomer of Freyssinet was employed to transfer the axial load to the top of the column. It is composed of a Teflon block-support and a sliding plate which was connected to the static jack. The principal characteristic of this support was to transmit the axial force continuously, permitting the lateral displacement of the top of the column. The dynamic jack-column connection was composed of a metallic cap, a mechanical screed, a metal rod, a ball joint, a universal joint and a connecting sleeve.

Automatic measurements were made using a computer, linked to Burr-Brown data acquisition system unit and Labtech Notebook software. This system enabled both the calibration of sensors and gauges, and visualization of the evolution of real-time parameters on the computer screen. The results (forces, displacements, and strains) were then treated using different programs to correct the parasitic effects of the system and to calculate the moments, curvatures, stiffness, dissipated energies and damping factors.

The forces transmitted by the static and dynamic jacks were measured by a load cell in the static jack and a pressure sensor in the dynamic jack. A digital voltmeter, installed on each jack control panel showed the load growth in real time at any moment. At the same time, the data acquisition system recorded the evolution of these forces automatically on a disk. The values of the applied lateral load were then corrected by deducting the friction force induced by the sliding support. The vertical load values were taken without further treatment.

The displacements were measured as follows:

• The displacements associated with the jacks were recorded using two LVDT sensors associated with dynamic and static jacks.

• The displacements at the top and at 2/3 of the height of the column, in the two principal axes of inertia, were recorded with LVDT RDP D5-2000 sensors.

• The displacements at 1/3 of the height of the column, in the two principal axes of inertia, were recorded with LVDT RDP D5-1000 sensors.

Measurement of the strains of the reinforcements was performed employing FL-5-11 gauges. To calculate the associated curvatures, three gauges per column were used so as to record two measurements of strains of the longitudinal reinforcements in each of the main axes of the column.

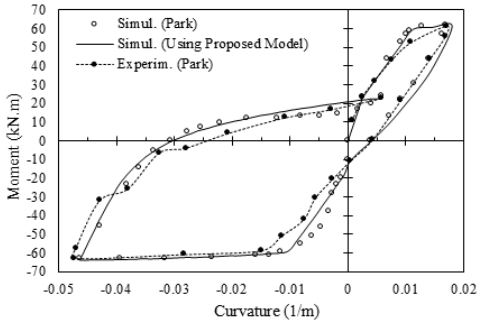

Fig. 5 Moment-curvature response, cyclic combined loading case

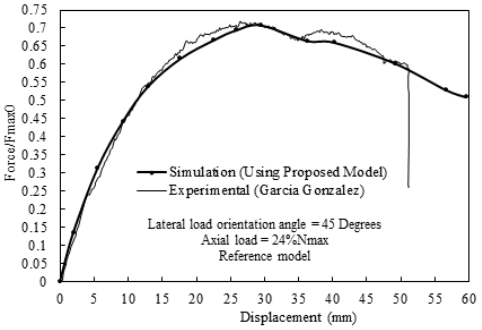

Fig. 6 Force-displacement response of the reference model, MLOLAF, $\Omega = 45^{\circ}$

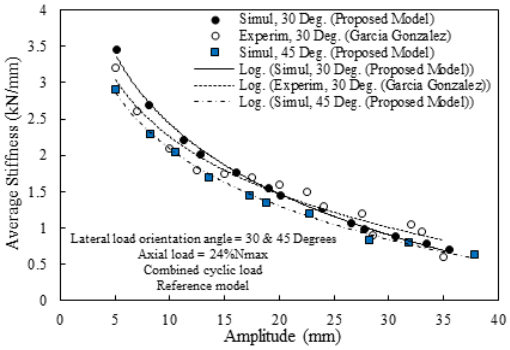

Fig. 7 Average stiffness, CLOLAF, $\Omega = 30^{\circ}$ and 45°

Park *et al.* (1972) performed a test on rectangular RC 1D SM under a cyclic combined loading. They tested a 1D SM under cyclic monoaxial bending moment and a compression axial loading of 160 kN, having a section of 30.5 cm×15.2 cm with four longitudinal reinforcement of type mild steel with yielding stress of 345 MPa and steel percentage of 2.4% (ρ = 2.4%). The used concrete had a compression ultimate stress of 34 MPa. See Fig. 5 for the moment-curvature response of the tested RC member.

5. Verification of the proposed algorithm

Figs. 5 to 8 demonstrate the comparison of the results

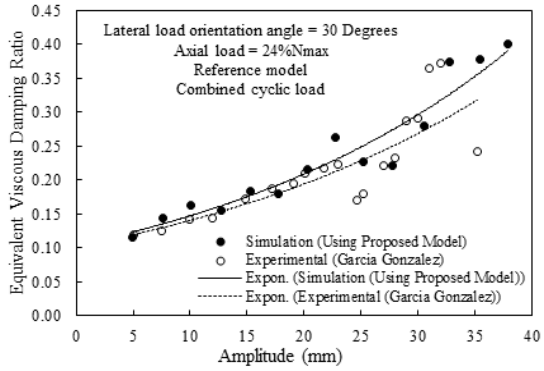

Fig. 8 Equivalent viscous damping ratios (EVDR), CLOLAF, $\Omega = 30^{\circ}$

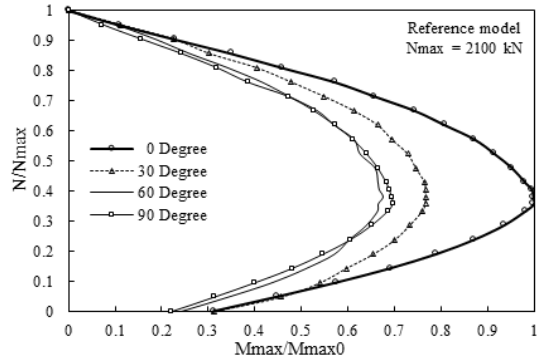

Fig. 9 Interaction diagram of reference section, MLOLAF, different Ω

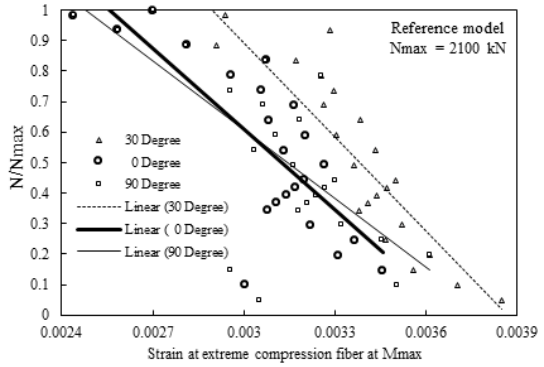

Fig. 10 Ultimate strain at extreme compression fiber "ε_u", MLOLAF

obtained from the numerical simulation applying the proposed algorithm and the experimental test results. As can be seen from these figures, there is a close agreement between the simulation (using the proposed algorithm) and the experimental test results.

Fig. 5 shows the comparison of the results obtained from the proposed simulation and the experimental test/simulation of Park *et al.* (1972) performed on an RC 1D SM subjected to cyclic combined loading. For the sake of clarity, only the first cycle of loading is shown in this figure.

Fig. 6, shows the comparison of the results obtained from the proposed simulation and the experimental test of Garcia Gonzalez (1990) on the reference model under MLOLAF with the orientation of $\Omega = 45°$.

In Figs. 7 and 8, the results of the proposed simulation and the experimental test of Garcia Gonzalez (1990) for the average stiffness and equivalent viscous damping ratio (EVDR) for CLOLAF, are compared.

As illustrated in Fig. 7, the logarithmic trendline type matches very well with the variation of stiffness. For the reference columns under CLOLAF the simulation give the following relation for the average stiffness for the orientation of loading of $\Omega = 30°$

$$Kav. = 5.63 - 1.39\ln(a) \tag{75}$$

And gives the following relation for the orientation of loading of $\Omega = 45°$

$$Kav. = 4.70 - 1.14\ln(a) \tag{76}$$

Where:

$Kav.$: Average stiffness in kN/mm,

a: Amplitude in mm.

In Fig. 8, the exponential trendline type matches very well with the variation of EVDR.

For the reference column under CLOLAF the simulation gives the following relation for the EVDR "ξ" for the orientation of loading of $\Omega = 30°$

$$\xi = 0.1\exp(0.035a) \tag{77}$$

Where:

a: Amplitude in mm.

6. Interaction diagram

Fig. 9 illustrates the normalized axial force-bending moment interaction diagram of the reference section subjected to different applied lateral force orientations. The ultimate resisting moments of the section (Mmax) under different axial loads and the lateral loads in different orientation angles are normalized to the maximum ultimate resisting moment of the section when the lateral load is applied in the direction of the main axis of the section (Mmax0). This figure illustrates that in the reference section, for all orientations, the balance point occurs when the applied axial force is about 38% of Nmax. At the balance point, the increase of the ultimate resisting moment is about 320%, 245%, 305% and 315% compared to the case of no axial load is applied for the lateral load orientations of 0°, 30°, 60° and 90°, respectively. Among these values, the minimum enhancement of ultimate strength occurs when Ω = 30°, while for the other cases the ultimate strength of the section is enhanced by a factor of more than three. In general, the minimum enhancement of the ultimate strength of the section due to axial force is observed when the lateral load is applied in the direction of the diagonal of the section (the diagonal orientation of reference section is Ω = Tan^{-1} (h/b) = 36°). The enhancement factor due to axial load for all of the lateral load orientations, ranges between 2.4 and 3.2.

7. Evolution of ultimate strain at extreme compression fiber (ε_u)

In Fig. 10, the evolution of ultimate strain at extreme

compression fiber ε_u (at the corner C) of a rectangular RC section due to the ultimate moment versus applied normalized axial force (N/Nmax) for three different orientations of lateral loading are shown. As the obtained results and their linear adapted trendlines show, strain decreases with increasing the axial force and it generally, ranges from 0.0024 to 0.0038. Therefore, the 0.003 value given by ACI-318 code for maximum strain in the design in extreme compression fiber, is not conservative and valid for the combined load cases with significant values of axial force (i.e., when N/Nmax > 0.70).

8. Conclusions

An algorithm together with a finite element computer program has been proposed to simulate numerically the nonlinear behavior of RC 1D SMs under combined loading, CLOLAF and MLOLAF as well as monotonic or cyclic BBMAL. The proposed algorithm has been validated by experimental test data. The interaction diagrams for rectangular sections under different lateral load orientations indicates that an axial force increases the strength of 1D SM up to the "balance point" for any lateral load orientation angle at approximately the same value of the axial load.

The evolution of ultimate strain at extreme compression fiber of a rectangular RC section due to the ultimate moment and applied normalized axial force for different orientations of lateral loading shows that the ultimate strain decreases with increasing the axial force. In the examined cases, this ultimate strain ranges from 0.0024 to 0.0038. Therefore, the 0.003 value given by ACI-318 code for ultimate strain, is not conservative and valid for the combined load cases with significant values of axial force (i.e., when N/Nmax > 0.70).

Acknowledgments

The technical and financial support of the Ecole Centrale de Nantes/France and the Near East University/Cyprus are appreciated.

References

Amziane, S. and Dubé, J.F. (2008), "Global RC structural damage index based on the assessment of local material damage", *J. Adv. Concrete Technol.*, **6**(3), 459-468.

CEB Code (1978), *Code-Modèle CEB-FIP Pour les Structures en Béton*, Bulletin d'information No. 124-125F, Comité Euro-International du Béton, Vol. 1 and 2, Paris, France.

Garcia Gonzalez, J.J. (1990), "Contribution á l'étude des poteaux en béton armé soumis á un cisaillement dévié alterné", Ph.D. Dissertation, University of Nantes/Ecole Centrale de Nantes, Nantes, France.

Hashemi, S.SH. and Vaghefi, M. (2015), "Investigation of bond slip effect on the P-M interaction surface of RC columns under biaxial bending", *Sci. Iran. Trans. A*, **22**(2), 388-399.

Lavassani, H.H., Tasnimi, A.A. and Soltani, M. (2009), "A complete hysterical constitutive law for reinforced concrete under earthquake loadings", *J. Seismol. Earthq. Eng.*, **11**(1), 17-40.

Mashaly, E-S, El-Heweity, M., Abou-Elfath, M. and Ramada, M. (2011), "A new beam-column model of seismic analysis of RC frames-part I: Model derivation", *Alexandr. Eng. J.*, **5**(4), 313-320·

Massumi, A. and Badkoubeh, A.R. (2015), "Dimensionless analysis of composite rectangular and circular RC columns", *Steel Compos. Struct.*, **19**(2), 327-348.

Massumi, A. and Monavari, B. (2013), "Energy based procedure to obtain target displacement of reinforced concrete structures", *Struct. Eng. Mech.*, **48**(5), 681-695.

Morfidis, K., Kiousis, P.D. and Xenidis, H. (2014), "A nonlinear model for ultimate analysis and design of reinforced concrete structures", *Comput. Concrete*, **14**(6), 695-710.

Norris, C.H. and Wilbur, E.J.B. (1974), *Elementary Structural Analysis*, 2nd edition, McGraw Hill Book Company, New York, U.S.A.

Parate, K. and Kumar, R. (2016), "Investigation of shear strength models for exterior RC beam-column joint", *Struct. Eng. Mech.*, **58**(3), 475-514.

Park, R., Kent, D.C. and Sampson, R.A. (1972), "Reinforced concrete members with cyclic loading", *J. Struct. Div.*, **98**(ST7), 1341-1359.

Pham, B.H., Davenne, L., Brancherie, D. and Ibrahimbegovic, A. (2010), "Stress resultant model for ultimate load design of reinforced-concrete frames: Combined axial force and bending moment", *Comput. Concrete*, **7**(4), 303-315.

Priestley, M.J.N. and Park, R. (1991), "Strength and ductility of concrete bridge columns under seismic loading", *ACI Struct. J.*, **88**(4), 61-76.

Sadeghi, K. (1995), "Simulation numérique du comportement de poteaux en béton armé sous cisaillement dévié alterné", Ph.D. Dissertation, University of Nantes/Ecole Centrale de Nantes, Nantes, France.

Sadeghi, K. (2001), *Numerical Simulation and Experimental Test of Compression Confined and Unconfined Concrete*, Technical Report Submitted to Water Resources Management Organization, Ministry of Energy, Concrete Laboratory of Power and Water University of Technology, Tehran, Iran.

Sadeghi, K. (2011), "Energy based structural damage index based on nonlinear numerical simulation of structures subjected to oriented lateral cyclic loading", *Int. J. Civil Eng.*, **9**(3), 155-164.

Sadeghi, K. and Nouban F. (2016), "Damage quantification and fatigue of RC structures", *Structu. Eng. Mech.*, **58**(6), 1021-1044.

Sadeghi, K. and Nouban F. (2017), "Behavior modeling and damage quantification of confined concrete under cyclic loading", *Struct. Eng. Mech.*, **61**(5), 625-635.

Sharma, M.R., Singh, A.K. and Benipal, G.S. (2014), "Stability of concrete beam-columns under follower forces", *Lat. Am. J. Sol. Struct.*, **11**(5), 790-809.

Sheikh, S.A. (1982), "A comparative study of confinement models", *ACI J.*, ***79***(4), 296-305.

Tasnimi, A.A. and Lavasani, H.H. (2011), "Uniaxial Constitutive Law for structural concrete members under monotonic and cyclic loads", *Sci. Iran. Trans. A*, **18**(2), 150-162.

Yau, C.Y., Chan, S.L. and So, A.K.W. (1993), "Biaxial bending of arbitrarily shaped reinforced concrete columns of arbitrary shape", *Struct. J. ACI*, **90**(3), 269-273.

Yen, J.Y.R. (1991), "Quasi-Newton method for reinforced concrete column analysis and design", *J. Struct. Struct. Div.*, **117**(3), 657-666.

CC